ACS APPLIED MATERIALS & INTERFACES

Article

Janus mesoporous silica nanoparticles for dual-targeting for tumoral cells and mitochondria.

Victoria Lopez, Maria Rocio Villegas, Veronica Rodríguez, Gonzalo Villaverde, Daniel Lozano, Alejandro Baeza, and María Vallet Regí

ACS Appl. Mater. Interfaces, **Just Accepted Manuscript** • DOI: 10.1021/acsami.7b06906 • Publication Date (Web): 31 Jul 2017

ACS Publications

ACS Applied Materials & Interfaces is published by the American Chemical Society. 1155 Sixteenth Street N.W., Washington, DC 20036

Janus Mesoporous Silica Nanoparticles for Dual-Targeting for Tumoral Cells and Mitochondria.

Victoria López,[a,†] Maria Rocío Villegas,[a,b,†] Verónica Rodríguez,[a] Gonzalo Villaverde,[a,b] Daniel Lozano,[a,b] Alejandro Baeza[a,b] and María Vallet-Regí*[a,b]*

a. Departamento de Química Inorgánica y Bioinorgánica, Facultad de Farmacia, Universidad Complutense de Madrid, 28040 Madrid, Spain.

b. Networking Research Center on Bioengineering, Biomaterials and Nanomedicine (CIBER-BBN), Av. Monforte de Lemos, 3-5. 28029 Madrid, Spain.

KEYWORDS

Janus Nanoparticles, Targeted nanosystems, Nanoocoloy, Mesoporus Silica Nanoparticles, mitochondria targeting.

ABSTRACT

The development of targeted nanocarriers able to be selectively internalized within tumoral cells and therefore, to deliver antitumoral drugs specifically to diseased cells, constitutes one of the most important goals in nanooncology. Herein, the development of Janus mesoporous silica particles asymmetrically decorated with two targeting moieties, one of them selective to folate membrane cell receptors (folic acid) and the other one able to bind to mitochondria membrane

(triphenylphospine) is described in order to achieve a sequential cellular to organelle vectorization. The asymmetric decoration of each side of the particle allows a finest control in the targeting attachment process in comparison with the use of symmetric nanocarriers. The presence of folic acid induces a higher increase in particle accumulation inside tumoral cells and once there, these nanocarriers are guided close to mitochondria by the action of the TPP moiety. This strategy can be applied for improving the therapeutic efficacy of current nanomedicines.

INTRODUCTION

The paramount discovery carried out in 1986 by Maeda and Matsumura about the natural tendency of nanometric systems to be passively accumulated within solid tumors[1] triggered the race to design nanocarriers able to deliver antitumoral agents specifically into diseased tissues.[2,3] Neoplastic tissues are irrigated by blood vessels which have been built in a chaotic way so that they usually exhibit fenestrations with diameters around a few hundred of nanometers.[4] Therefore, when the nanocarrier reaches the tumoral area, it is able to pass through these pores reaching the tumoral tissue whereas it cannot cross the healthy vessel walls. Additionally, the rapid expansion of tumoral cells compresses the nearby located lymphatic vessels compromising the drainage which enhances the accumulation time of nanocarriers into the diseased zone. This phenomenon, called EPR (*Enhanced Permeation and Retention*) effect, has also been so-called as primary targeting being the responsible for nanocarrier accumulation in tumoral tissues. However, this solely effect is not enough to achieve an improved therapeutic response over conventional therapy. Tumoral masses are incredibly complex tissues which are formed by a myriad of different cells (cancerous, supportive, immune cells and so on)[5] Therefore, the capacity to distinguish between malignant and healthy cells is necessary for improving the

effectiveness of nanomedicines. In order to acquire this property, the external surface of nanocarriers can be decorated with certain moieties such as antibodies,[6] aptamers,[7] vitamins,[8] peptides[9] or synthetic molecules,[10] which are recognized by specific membrane cell receptors overexpressed by the tumoral cells. The presence of these targeting agents (called secondary targeting) enhances the accumulation within the tumoral cell. Additionally, two targeting moieties can be anchored on the same nanocarrier in order to enhance even more the selectivity of the nanodevice.[11-13] It is also possible to control the nanoparticle trafficking within the cell placing targeting moieties able to recognize organelles such as mitochondria or cell nucleus (tertiary targeting).[14] Therefore, different tertiary targeting agents have been attached on drug loaded nanoparticles achieving significant improvements in the therapeutic efficacy of the transported payloads.[15] In sight of these results, the possibility to design systems which combines these targeting capacities (tissular, cellular and organelle) has aroused great attention in the scientific community for improving even more the capacity to destroy tumoral cells limiting the side effects and systemic toxicity of the therapy. Thus, it has been reported engineered peptides which carry specific cellular and organelle targeting devices,[16] nanoparticles doubly functionalized with both targeting agents[17] and also nanocarriers functionalized with hierarchical targeting devices which recognize specific membrane cellular receptors and certain organelles following an activatable tandem mechanism.[18] However, in many cases, they lack of a precise control in the targeting ratio, have low transport capacity or requires the synthesis of complex moieties. Recently, Ma and co-workers have carried out a computational study in order to determine the best configuration of the targeting moieties in dual-targeted nanocarriers concluding that Janus-type structures achieved the fastest engulfment by the cell membrane,

regardless the physicochemical properties and the separation between the targeting group and the carrier surface.[19]

Herein, we describe an easy procedure for the synthesis of Janus mesoporous silica nanoparticles (J-MSN) which carry two different targeting moieties, cell and organelle targeting moiety, respectively, each located in one hemisphere of the particle (Figure 1). Mesoporous silica nanoparticles (MSN) present great cargo capacity, excellent biocompatibility and easy and cheap production.[20,21] In the approach here presented, one of the hemisphere of MSN was decorated with folic acid which act as cellular targeting agent due to the fact that many tumoral cell lines usually overexpress folate receptor.[22] On the other hemisphere, a triphenylphospine derivative (TPP) was anchored for directing the nanocarrier to the mitochondria membrane exploiting the affinity of this positively charged group for the highly negative mitochondria membrane.[23] The efficacy of this device has been evaluated using human prostate cancer cells (LNCaP), which present higher expression of folate-binding proteins on their membrane.[24,25] This system showed an enhanced accumulation in tumoral cells in comparison with a control line composed by healthy pre-osteoblastic cells (MC3T3-E1) which do not present a overexpression of folate-binding proteins. Additionally, the presence of TPP on the particle surface leads to a selective accumulation of the nanoparticles close to mitochondria. Finally, when the carriers were loaded with topotecan (TOP), a potent DNA topoisomerase inhibitor which induces nuclear and mitochondria DNA damage,[26] the double targeted device exhibit significant higher toxicity in comparison with the particles decorated only with one of the targeting moieties, which point out that the TOP effect is stronger when it is released close to mitochondria. These results indicate that the use of J-MSN decorated with cellular and organelle targeting agents can significantly improve the efficacy of the transported drugs in antitumoral therapies.

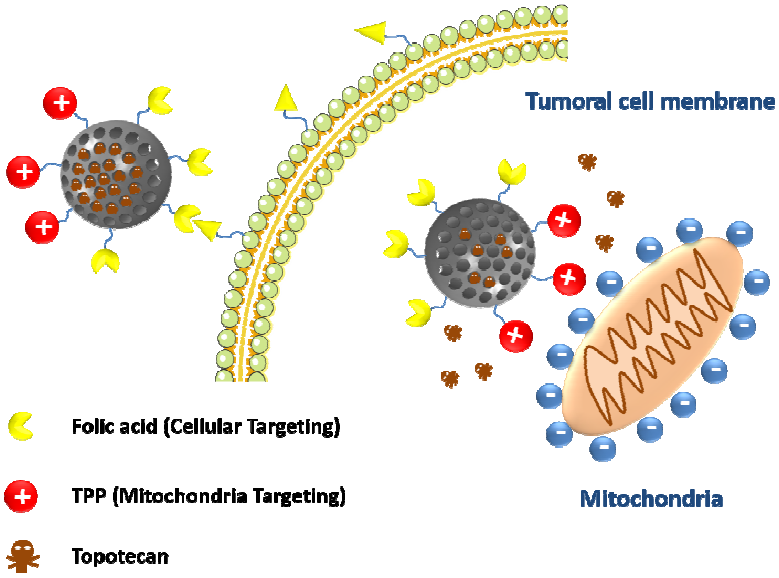

Figure 1. Mechanism of action of dual targeted MSN: cellular and mitochondria targeting.

EXPERIMENTAL SECTION

Materials and Methods

The following compounds were purchased from Sigma-Aldrich Inc.: aminopropyltriethoxysilane (APTES), ammonium nitrate, cetyltrimethylammonium bromide (CTAB), tetraethyl orthosilicate (TEOS), dicyclohexylcarbodiimide (DCC), *N*-hydroxysuccinimide (NHS), *N*-diisopropylethylamine (DIPEA), fluorescein isothiocyanate (FITC), folic acid, succinic anhydride, 4-carboxy-1-(triphenyl-l4-phosphanyl)butan-1-ylium bromide, topotecan hydrochloride hydrate (TOP, >98%) and trifluoroacetic acid (TFA). All other chemicals (absolute ethanol, DMF, DMSO, acetone, ethyl ether, dichloromethane (DCM), heptane, dry solvents etc.) were commercially available and of best quality and they were employed as received.

Characterization techniques

Fourier transform infrared spectroscopy (FTIR) was performed using a Thermo Nicolet nexus equipped with a Goldengate attenuated total reflectance device. The textural properties of the

materials were determined by nitrogen sorption porosimetry using a Micromeritics ASAP2010 instrument. Prior to perform the N_2 measurements, the samples were degassed under vacuum for 24 h at room temperature. Thermogravimetry analysis (TGA) was performed using a Perkin Elmer Pyris Diamond TG/DTA analyser with a 5 $^{o}C \cdot min^{-1}$ heating ramp from room temperature to 600 ^{o}C. The hydrodynamic size of the mesoporous nanoparticles was measured by means of a Zetasizer Nano ZS (Malvern Instruments) equipped with a 633 nm ‘‘red’’ laser. Mass spectra were acquired using a Voyager DE-STR Biospectrometry MALDI-TOF mass spectrometer. Scanning electron microscopy (SEM) analyses were performed on a JEOL 6400-LINK AN10000 microscope (Electron Microscopy Centre, UCM). The samples underwent the Au metallization prior to observation. Liquid NMR experiments were performed using a Bruker AV 250 MHz.

Synthesis of (2,2-dimethyl-4,15-dioxo-3,8,11-trioxa-5,14-diazanonadecan-19-yl)triphenylphosphonium bromide (TPP-NH_2)

To a solution of 4-carboxy-1-(triphenyl-l4-phosphanyl)butan-1-ylium bromide (250 mg) and *N*-hydroxysuccinimide (130 mg, 2 eq) in 3 mL of DMF, DIC (260mg, 3 eq) and DIPEA (1.2 mL, 6 eq) were added under inert atmosphere. The mixture was stirred during 4 hours at room temperature. When the acid activation was finished, a solution of tert-butyl (2-(2-(2-aminoethoxy) ethoxy)ethyl)carbamate (303 mg, 1.1 eq) was added dropwise. The mixture was stirred overnight. Crude was precipitated in cool ether and the filtrated solid was purified by flash column chromatography (chloroform/MeOH 4:1). The resulting product was characterized by 1H NMR (250 MHz, CDCl3) δ 8.24 (t, J = 5.3 Hz, 1H, NH, amide), 7.89 – 7.76 (m, 9H, TPP), 7.76 – 7.63 (m, 6H, TPP), 5.18 (s, 1H, NH-Boc), 3.72 (dd, J = 14.0, 7.0 Hz, 2H), 3.59 –

3.47 (m, 8H), 3.40 (dd, J = 11.9, 6.2 Hz, 2H), 3.34 – 2.61 (m, 1H), 2.70 – 2.57 (m, 1H), 2.03 – 1.84 (m, 2H, CH2), 1.80 – 1.55 (m, 6H, 3xCH2), 1.42 (s, 9H, 3xCH3, Boc).

The next step was the removal of Boc-protecting group which was carried out dissolving the product in 2 mL of DCM/TFA (1%) and stirring during two hours. Crude was precipitated in cool ether and the filtrated solid was purified by flash column chromatography (chloroform/MeOH 4:1). The resulting product was characterized by 1H NMR (250 MHz, CDCl3) δ 8.53 (bs, 2H, NH2), 8.23 (s, 1H, NH, amide), 7.89 – 7.76 (m, 9H, TPP), 7.76 – 7.63 (m, 6H, TPP), 3.85 (bs, 2H), 3.59 – 3.47 (m, 8H), 3.40 (bs, 2H), 3.21 (bs, 1H), 2.70 – 2.57 (m, 1H), 1.94 (m, 2H, CH2), 1.80 – 1.55 (m, 6H, 3xCH2).

Synthesis of fluorescent MSN

Prior, FITC (1 mg) and APTES (2.2 μL) were dissolved in the minimum volume of EtOH and the mixture was stirred at room temperature for 2 hours under a N_2 atmosphere. The resulting solution was called Solution 1.

MSN were synthesized as following: to a 1 L round-bottom flask, 1 g of CTAB as a structure-directing agent, 480 mL of H_2O (Milli-Q), 3.5 mL of NaOH (2 M) were added. The mixture was heated to 80ºC and stirred at 600 rpm. When the reaction mixture was stabilized at 80 ^oC, 5 mL of TEOS were mixed with solution 1 and the resulting solution was added dropwise at 0.33mL/min rate. The pale yellow suspension obtained was stirred during further 2h at 80 ^oC. The reaction mixture was filtered and washed 3 times with 100 mL of H_2O, and then ones with 50 mL of EtOH. Finally, the surfactant was removed by ionic exchange using a solution of amonium nitrate (10 $mg \cdot mL^{-1}$) in 400 mL of ethanol (95%) at 65 ^oC overnight with magnetic stirring under reflux. This procedure was repeated twice in order to eliminate completely the surfactant.

Synthesis of aminated mesoporous silica particles (MSN-NH_2)

200 mg of the dried MSN particles were vortexed during 80 seconds with a mixture of 1 g molten paraffin in 11.6 mL H_2O, 4.4 mL EtOH and 2 mg of CTAB at 70 ^oC. After this time, the suspension was immediately cooled down in order to solidify the paraffin. The obtained particles were filtered, washed and subsequently dispensed in 14 mL EtOH containing 1.5 mL NH3 (aq., 25%). After addition of 0.47 mL APTES (2 mmol), the mixture was shaken overnight on an orbital shaker at room temperature. The solid was filtered and washed with heptane until there was no paraffin residue measured by FTIR.

Uniformly aminated MSN were synthesized as control by the following synthetic procedure, TEOS (4.5 mL) and APTES (0.5 mL) were mixed and added dropwise to solution of 1 g of CTAB, 480 mL of water and 3.5 mL of 2 M NaOH at 80 ^oC. The final reaction mixture was stirred at 80 ^oC for 2 hours. A white solid was filtered and washed with water and EtOH.

Synthesis of carboxylic acid-functionalized particles (MSN-CO_2H)

200 mg of MSN-NH_2 particles were suspended in 10 mL of dry THF under N_2 gas as inert atmosphere. To this solution, 40 mg succinic acid was added and the mixture was stirred at room temperature overnight. The obtained particles were filtered and washed with THF.

Synthesis of amino-carboxylic acid particles (H_2N-MSN-CO_2H)

130 mg of MSN-CO_2H previously dried under vacuum were suspended in dry toluene under N_2 gas and 0.15 mL of APTES was added. The mixture was refluxed at 110 ^oC overnight under inert atmosphere. The obtained particles were filtered and washed with toluene and ethyl ether.

Synthesis of Folic-MSN-CO_2H

22 mg of folic acid (50 mmol) were dissolved in 2 mL of dry DMF/DMSO (4:1). 36 mg of DCC and 38 mg of NHS were added to this solution and the mixture was stirred at room

temperature during 30 min under N_2 atmosphere. After this time, the solution was added to a suspension of 50 mg of dried H_2N-MSN-CO_2H in 3 mL of DMF/DMSO (4:1). The resulting suspension was stirred under N_2 atmosphere overnight. The obtained particles were filtered and washed with DMF/DMSO (4:1), water and acetone.

Synthesis of H_2N-MSN-TPP

100 mg of H_2N-MSN-CO_2H were suspended in 2 mL of dry DMF which contain 12 mg of DCC and 13 mg of NHS. 41 mg of the TPP derivative were dissolved in 1 mL of dry DMF which contains 5 μL of DIPEA and this solution was added to the particle suspension. The resulting mixture was stirred overnight under N_2 atmosphere. The obtained particles were filtered and washed with DMF, water and acetone.

Synthesis of Folic-MSN-TPP

22 mg of folic acid (50 mmol) were dissolved in 2 mL of dry DMF/DMSO (4:1). 36 mg of DCC and 38 mg of NHS were added to this solution and the mixture was stirred at room temperature during 30 min under N_2 atmosphere. After this time, the solution was added to a suspension of 50 mg of dried H_2N-MSN-TPP in 3 mL of DMF/DMSO (4:1). The resulting suspension was stirred under N_2 atmosphere overnight. The obtained particles were filtered and washed with DMF/DMSO (4:1), water and acetone.

TOP loading within MSN derivatives

50 mg of each MSN (NH_2-MSN-CO_2H, MSN-Fol, MSN-TPP and Fol-MSN-TPP, respectively) were placed in a dark glass vial and dried at 80 ^oC under vacuum during 4 hours. After this time, 5 mL of an aqueous solution of TOP (3 mg·mL-1) were added and the suspension was stirred at room temperature for 48 h. The particles were filtered and the excess of TOP was removed by washing three times with water. The amount of drug loaded in each system

was determined from the difference between the fluorescence measurements of the initial and recovered solutions (λ_{exc}= 400, λ_{em}=540 nm). In all the cases, the amount of TOP loaded was around 5% in weight.

Cell cultures

Cell culture studies were performed using mouse osteoblastic cell line MC3T3-E1 (subclone 4, CRL-2593; ATCC, Mannassas, VA) and androgen-sensitive LNCaP cells, a human prostate cancer cell line (CRL-1740; ATCC, Mannassas, VA). The tested MSNs (6 μg/mL) were placed into each well of 6- or 24-well plates (CULTEK) after cell seeding. MC3T3-E1 and LNCaP cells were then plated at a density of 20.000 cells·cm^{-2} in 1 mL of alfa-minimum essential medium or Dulbecco's modified Eagle's medium (DMEM, Sigma Chemical Company), respectively, containing 10% of heat-inactivated fetal bovine serum and 1% penicillin (BioWhittaker Europe)–streptomycin (BioWhittaker Europe) at 37 ºC in a humidified atmosphere of 5% CO_2, and incubated for different times. Some wells contained no MSNs as controls.

Nanoparticle uptake studies by flow cytometry

After 24h, the cells were incubated in the absence or presence of the tested MSNs (6μg/mL) during 2 hours. Cells were then washed twice with PBS and incubated at 37 ºC with trypsin–EDTA solution for cell detachment. The reaction was stopped with culture medium after 5 min and cells were centrifuged at 1.500 rpm for 10 min and resuspended in fresh medium. Then, the surface fluorescence of the cells was quenched with trypan blue (0.4%) to confirm the presence of an intracellular, and therefore internalised, fluorescent signal. Flow cytometry measurements were performed at an excitation wavelength of 488 nm, green fluorescence was measured at 530 nm (FL1). The trigger was set for the green fluorescence channel (FL1). The conditions for the data acquisition and analysis were established using negative and positive controls with the

CellQuest Program of Becton–Dickinson and these conditions were maintained during all the experiments. Each experiment was carried out three times and single representative experiments are displayed. For statistical significance, at least 10,000 cells were analyzed in each sample in a FACScan machine (Becton, Dickinson and Company, USA) and the mean of the fluorescence emitted by these single cells was used.

Nanoparticle uptake studies by fluorescence microscopy

Cells were incubated with the MSNs (6μg/mL) for 2h in serum-free culture medium. Then, the medium was withdrawn and cells were washed with PBS three times. Cells were incubated for 45 minutes with MitoTracker® to stain mitochondria. Cells were washed, fixed with ethanol for 2 min and stained with DAPI (40, 60 diamidino-2-phenylindole) at 1μg/mL. Fluorescence microscopy images were taken to evaluate MSNs. Green channel was used to locate for MSNs, blue for cell nucleus and red for mitochondria in a Evos FL Cell Imaging System equipped with tree Led Lights Cubes (lEX (nm); lEM (nm)): DAPI (357/44; 447/60), GFP (470/22; 525/50), RFP (531/40; 593/40) from AMG (Advance Microscopy Group).

Cell viability after incubation with Topotecan-loaded MSN

Cell growth was analyzed using the CellTiter 96AQueous Assay (Promega, Madison, WI, USA), a colorimetric method for determining the number of living cells in culture. Briefly, both type of cells were cultured as described above without (control) or with the corresponding amount of functionalized MSNs (100 $\mu g \cdot mL^{-1}$) and TOP-loaded MSNs (6 $\mu g \cdot mL^{-1}$), during 24 hours and 6 hours respectively. In the case of empty MSN, the cells were analyzed after the incubation time. In the case of TOP-loaded MSN, after the 6 hours incubation time, cells were gently washed two times with PBS and they were incubated in cell culture medium during 48h more. 40 μL of CellTiter 96 AQueous One Solution Reagent (containing 3-(4,5-dimethythizol-2-

yl)-5-(3-carboxymethoxyphenyl)-2-(4-sulfophe-nyl)-2H-tetrazoliumsalt (MTS) and an electron coupling reagent (phenazine ethosulfate) that allows its combination with MTS to form a stable solution) was added to each well and incubated for 4h. The absorbance at 490 nm was then measured in a Unicam UV-500 UV–visible spectrophotometer.

RESULTS AND DISCUSSION

MSN were prepared following a previously reported modified Stöber method which incorporates fluorescein covalently attached within the silica matrix.[27] The presence of this fluorophore is required in order to allow the easy monitorization of nanoparticle cell uptake by fluorescence microscopy and cytometry techniques. There are different strategies for the asymmetric functionalization of this type of mesoporous materials.[28] In our case, MSN were decorated with amino groups on one hemisphere following a two-step process which employs wax-in-water Pickering emulsions.[29,30] In this method, silica particles were added over a vigorously stirred aqueous emulsion of paraffin above the melting temperature of the wax (53-57 ^{o}C). After a short stirring time, the mixture was rapidly cooled at room temperature and the paraffin solidifies trapping the MSN particles on the surface (Figure 2b-c). The exposed MSN surface was functionalized with aminopropyltriethoxysilane (APTES) and finally, the paraffin was removed washing with heptane. Following this method, fluorescent round-shaped MSNs (MSN-NH_2) with size distribution centred on 190 nm as can be observed by transmission electron microscopy (TEM) were obtained (Figure 2d). In order to study the asymmetrization process, MSN-NH_2 were mixed with gold nanoparticles (5 nm of diameter) in aqueous solution during 12 hours. After this time, the suspension was centrifuged at mild condition (5000 rpm and 10 min) and the isolated particles were observed by TEM showing that the gold nanoparticles

were mainly located on one side of MSN due to the affinity of gold by amino groups which confirmed the asymmetric nanoparticle decoration (Figure 2e). When the same experiment was carried out with naked particles (MSN) the gold nanoparticles were not adsorbed on the silica surface remaining in the solution (Figure S1). Additionally, the percentage of nanoparticles which exhibited Janus structure was statistically determined by collecting several sets of TEM images showing that around 66% of particles were asymmetrically functionalized with amino groups (Figure S2 and Table S1 in supporting info). MSN completely decorated with amino groups were synthesized and treated with the gold nanoparticles in order employ them as control. In this case, the gold nanoparticles were uniformly distributed around the practically all the MSN (96%) which indicated a uniform distribution of the amino groups (Figure S3 and Table S1 in supporting information). Finally, the asymmetrization process was also confirmed by the hydrophilicity change in the particles after the introduction of amino groups which was monitored placing the particles in a vial which contains the same amount of an aqueous PBS solution (pH = 7.4) and dichloromethane. The particles uniformly functionalized with APTES, which are more hydrophobic, are located in the organic phase whereas the hydrophilic naked particles are placed in the aqueous phase. In the case of MSN-NH_2, they are mainly placed in the interphase, which proved the dual nature of these particles (Figure S4). All these data support the good performance of the asymmetrization process and are in agreement with previously reported works.[29,30]

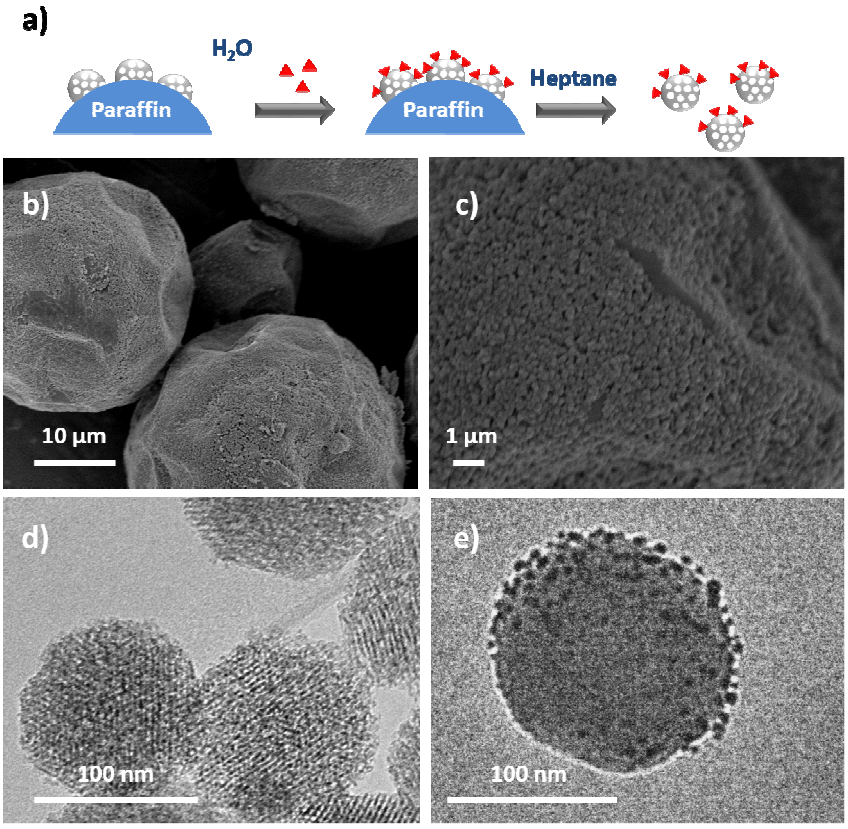

Figure 2. a) Scheme of asymmetrization pathway of MSN (red triangles represent APTES which is employed as amino source) b-c) SEM image of paraffin beads with MSN embedded, d) TEM image of MSN-NH_2 and e) TEM image of gold nanoparticles on one side of MSN-NH_2.

The asymmetrization process did not alter the particle morphology but it induced a slight hydrodynamic diameter increase (from 160 to 190 nm) according with dynamic light scattering (DLS) (Figure S5). Zeta potential measurement of the particles in phosphate buffer solution (pH 7.2) showed a drastic change in surface charge, from negative value (-20,5 mV) of the naked particles to positive one (+22.4 mV) of aminated nanoparticles (Figure 3). This change confirms the presence of amino groups on the particle surface, because they are protonated at physiological pH. The precise amount of amino groups was determined by quantitative Fmoc protocol[31] yielding a result of 100-130 µmol of amino groups per gram of MSN-NH_2. In order to

attach the targeting agents each of them in a hemisphere of the particle, anchoring points with different reactivity should be incorporated in each side. Amino and carboxylic groups were selected because there are many synthetic procedures for grafting biomolecules to them.[32] Therefore, the amino groups present in MSN-NH_2 were derivatised to carboxylic acid by their reaction with succinic anhydride in organic solvent. Then, the remained silanol groups present in the free hemisphere of MSN-CO_2H were react with APTES in order to introduce amino groups in the other side yielding the asymmetrically functionalized NH_2-MSN-CO_2H (Scheme 1).

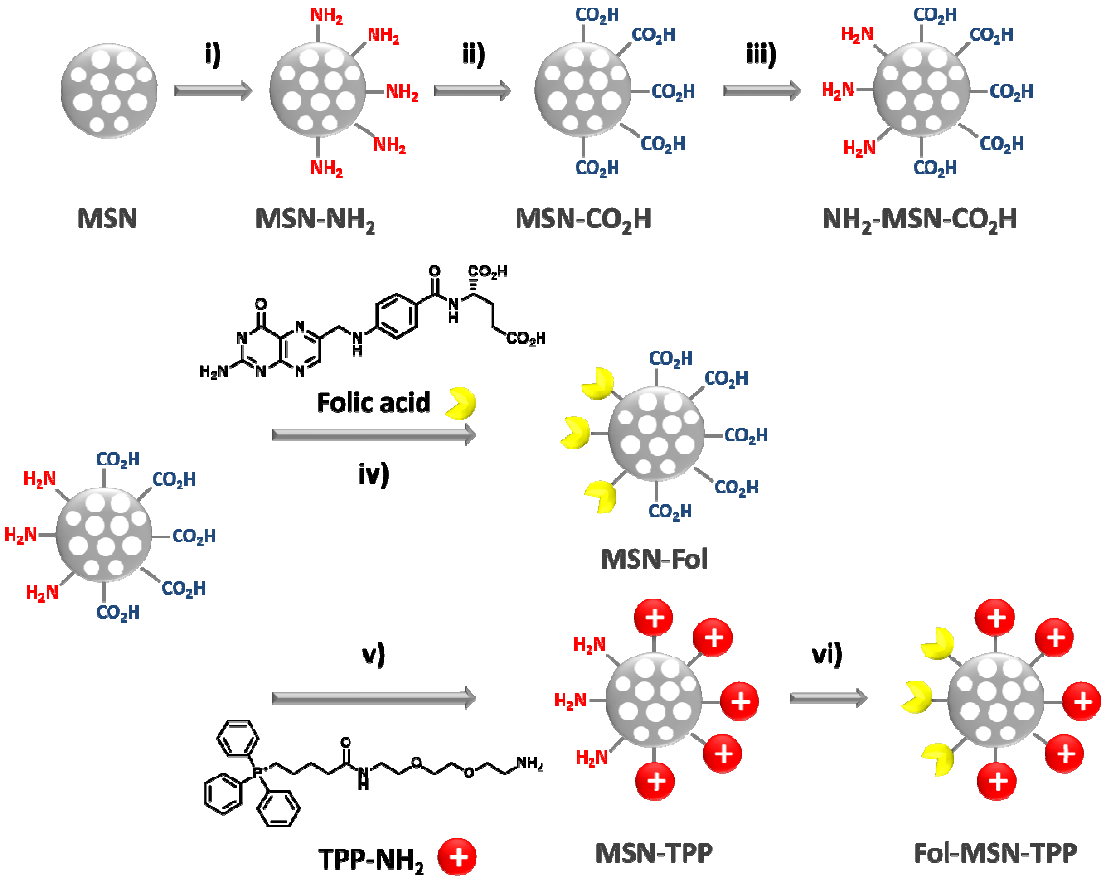

Scheme 1. Synthetic pathway for the synthesis of asymmetrically functionalized MSN, i) Paraffin/CTAB/EtOH/H2O/NH3 (aq)/APTES, ii) succinic ahydride/THF, iii) APTES/Toluene/reflux, iv) DMF/DMSO/DCC/NHS, v) DMF/DCC/NHS/DIPEA and vi) DMF/DMSO/DCC/NHS.

The complete synthetic process was monitored by Zeta potential measurements (Figure 3). The transformation of the amino groups of MSN-NH_2 into carboxylic groups leads to a strong decrease in the positive charge (MSN-CO_2H) which is partially re-established when new amino groups are introduced in the free hemisphere (NH_2-MSN-CO_2H). The attachment of folic acid was carried out in the NH_2 side employing the well-known carbodiimide chemistry. The carboxylic group of the folic acid was activated by reaction with dicyclohexylcarbodiimide (DCC) and *N*-hydrosuccinimide (NHS) and then, the resulting ester was directly added to a suspension of NH_2-MSN-CO_2H yielding MSN-Fol. After this step, the surface charge of the particle changed back to negative value which is the consequence of the reduction of free amino groups on the particle surface. In the case of the attachment of TPP moieties, a specific TPP analogue which carry one amino group at the end (TPP-NH_2) was synthesized (see experimental section for more details). These TPP moieties were introduced following a similar procedure but, in this case, through the activation of the carboxylic groups of NH_2-MSN-CO_2H with DCC and NHS followed by the subsequent addition of TPP-NH_2. As it was expected, surface charge suffered a significant increase after this synthetic step due to the introduction of positive charges on the particle surface. Finally, Folic acid was anchored to the free amino groups of MSN-TPP leading to a dramatic reduction of the charge. Additionally, the introduction of each targeting agent was confirmed measuring the amount of organic material by thermogravimetric analysis, before and after the grafting step (Table below Figure 3) and also by FTIR spectroscopy, which shows the apparition of characteristic bands after each synthetic step (Figure S6).

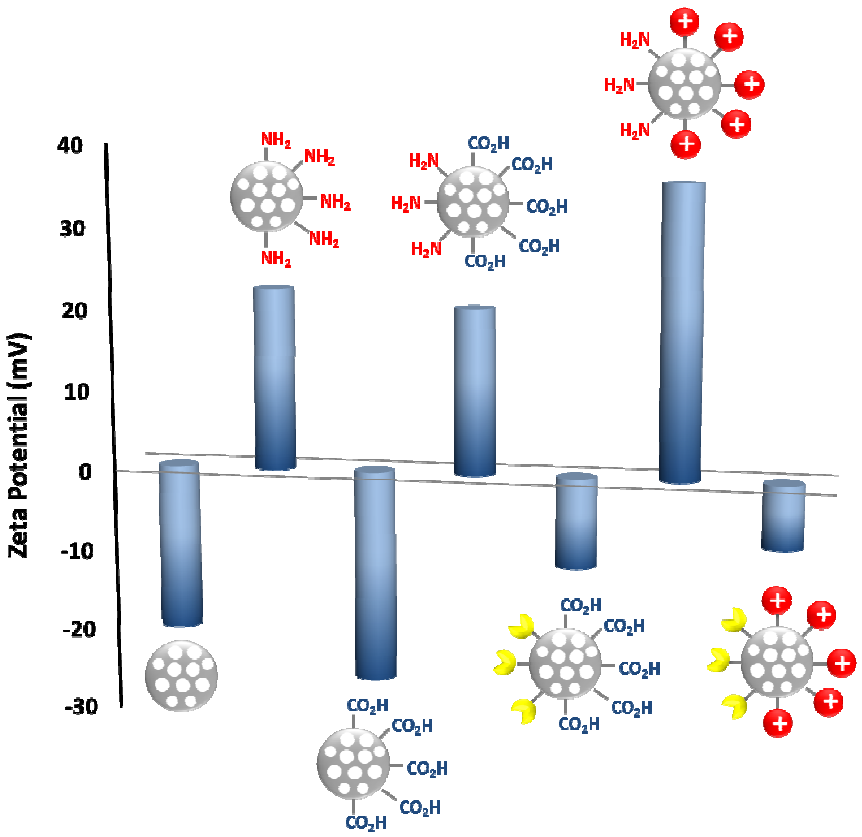

	MSN-Fol	MSN-TPP	TPP-MSN-Fol
$\%\Delta W_{organic\ material}$ *	8	3	12

Figure 3. Upper figure represents Zeta potential measurements of functionalized MSN derivatives. Lower Table shows the increment in amount of organic material after the grafting step (*).

Human prostate cancer cells (LNCaP) were selected as tumoral model cell line due to the overexpression of folate-binding receptors on their membrane.[24,25] In order to evaluate the capacity to enhance the particle uptake of each targeting agent, separately and asymmetrically combined in one single particle, LNCaP cells were exposed to a fixed concentration (6 $\mu g \cdot mL^{-1}$) of each type of fluorescently labeled (in green) nanoparticles: NH_2-MSN-CO_2H, MSN-Fol, MSN-TPP and Fol-MSN-TPP respectively during 2 hours. After this time, the cells were gently

washed with PBS in order to remove non internalized particles. The number of cells which had engulfed fluorescent nanoparticles was determined by flow cytometry. In order to discard the particles which are simply attached on the cell membrane and not internalized inside, the external fluorescence was quenched adding trypan blue before cell counting. Thus, only the cells which have particles inside the inner space are counted as positive. The same experiment was carried out in parallel using healthy pre-osteoblastic cells (MC3T3-E1), as model of cells which does not overexpress folate binding proteins on their surface, in order to evaluate the capacity of these nanocarriers to distinguish between tumoral cells and healthy ones. In the case of tumoral cells, the uptake was around 25% when the particles did not present any targeting moiety (NH_2-MSN-CO_2H) whereas this value doubles when the particles were decorated with folic acid on one hemisphere (Figure 4). Interestingly, particles functionalized only with TPP (MSN-TPP) almost triplicate the uptake in comparison with the untargeted particles, showing than 63% of the tumoral cell population engulfed these nanosystems, which are higher than the uptake achieved with the particles decorated with folic acid. The reason could be that these nanoparticles presented the highest positive charge at physiological pH and therefore, they present strong affinity by the negatively charged tumoral cell membrane. In any case, nanoparticles decorated with both targeting moieties (Fol-MSN-TPP) showed the highest uptake value (more than 90%) which indicates that the presence of these groups significantly enhances the uptake in this tumoral cell line. Regarding the nanoparticle uptake observed in healthy cells, only 10 % of the untargeted MSNs were captured by the cells while this value was significantly higher in the case of folic and TPP monofunctionalized MSN (Figure 4). Obviously, healthy cells also express folate receptors on their surface (although in lesser amount than tumoral cells) because this vitamin is essential and it participates in many biochemical pathways such as amino acids

metabolism and synthesis of RNA and DNA, among others. For this reason, the uptake of folic-functionalized MSN was higher than untargeted MSN but it was lower than in the case of tumoral cells. Similar uptake has been yielded with MSN-TPP. This fact can be explained as in the previous case due to the electrostatic affinity between the positively charged nanoparticles and the negatively charged cell membrane. Finally, the uptake of dual targeted MSN was slightly higher than the observed in mono-functionalized ones, but it was notably lower than the uptake achieved by tumoral cells (52% in healthy cells versus 91% in the case of tumoral cells). These results indicate the capacity of dual-targeted MSN to reach the inner space of tumoral cells in a selective manner which reflects its potential suitability for antitumoral therapy.

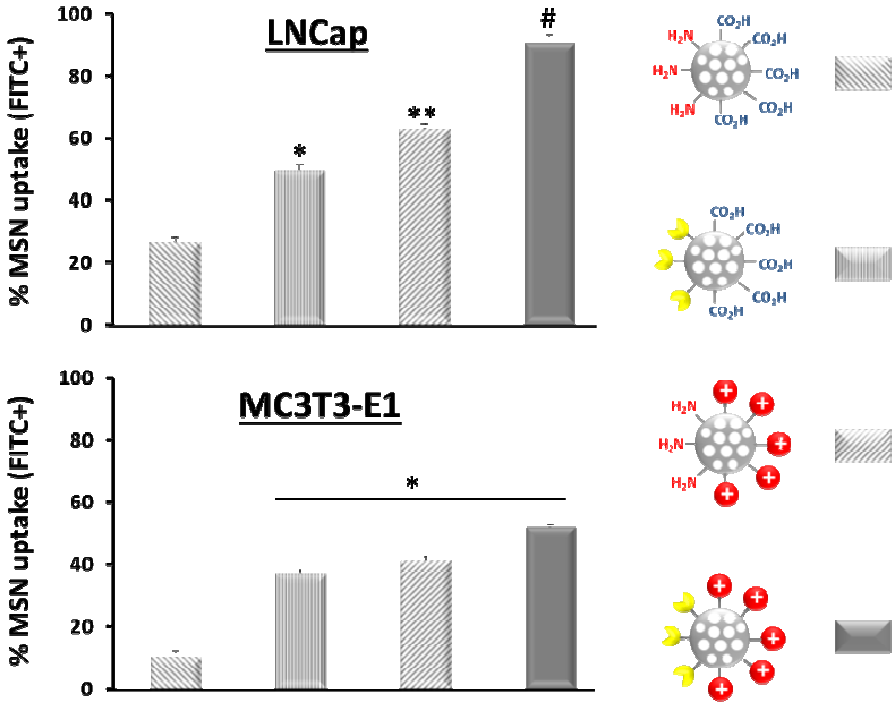

Figure 4. Comparative nanoparticle uptake of MSN derivatives in LNCaP and MC3T3-E1 cell lines, respectively, and 2 hours of exposition time. Data are mean ± SEM of 3 independent experiments performed at least in triplicate *p < 0.05 vs. NH2-MSN-CO2H; **p < 0.05 vs. MSN-Fol and NH2-MSN-CO2H; #p < 0.05 vs. all conditions (Student's t-test).

In order to study with more detail, the particle fate within the tumoral cell as well as the efficacy of the organelle targeting moiety, cells were incubated with each type of nanoparticle in the same conditions and then, they were stained with blue DAPI as nuclei tracker and red Mitotracker® for labeling mitochondria. This staining protocol allows the qualitative determination by fluorescent microscopy of the particle location within the cells, detecting each fluorophore in separate channels, as has been reported elsewhere.[33] In both cell lines, untargeted MSN were barely uptaked by the cells (Figure 5a and c). MSN-Fol showed higher uptake but significantly lower than the internalization achieved with MSN-TPP (Figure 5 b and d, versus e and g). Moreover, in the last case the presence of TPP on the particle surface caused that the nanoparticles were placed in close proximity with mitochondria, as can be observed by the overlapping between the green spots associated to the fluorescein of the nanoparticles and the red ones due to the mitochondria staining agent. Finally, dual-targeted MSN exhibited the highest accumulation and mitochondria localization in both cell lines (Figure 5 f and h) being higher in the case of tumoral cell line, which confirms the results obtained by flow cytometry.

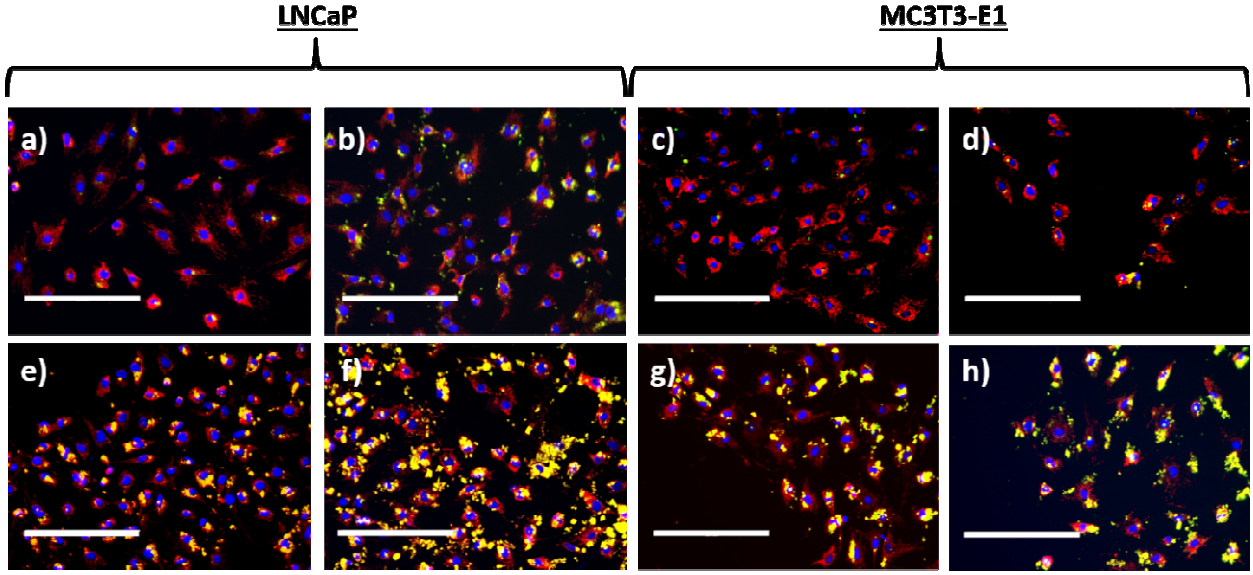

Figure 5. Fluorescence microscopy images of cells exposed to a fixed concentration of the following MSN derivatives: NH_2-MSN-CO_2H a) and c), MSN-Fol b) and d), MSN-TPP e) and g), Fol-MSN-TPP f) and h). Blue color corresponds to cell nuclei, obtained using blue DAPI staining agent, red color corresponds to mitochondria, obtained employing red MitoTracker® and green dots correspond to MSN nanosystems due to the presence of fluorescein trapped within the silica matrix (White scale bars correspond to 200μm).

The use of nanodevices as drug carriers for clinical applications requires that the designed material present excellent biocompatibility and absence of cytotoxicity. MSN is a biocompatible material which presents low toxicity, lack of immunogenicity and is degraded into non-toxic compounds (mainly silicic acid) in relatively short time periods.[34] Despite its lack of toxicity, the surface modification of this material could provoke the apparition of toxicity due to the enhanced uptake within the cells. In order to evaluate the absence of toxicity, LNCaP and MC3T3-E1 cells were incubated with a significantly higher amount of functionalized MSNs (100 μg·mL-1) in cell culture medium during 24 hours. After this time, cell viability was determined using the standardized cell viability test by MTS reduction. The results showed that none of these empty materials exhibited cytotoxicity in both cell lines (Figure 6).

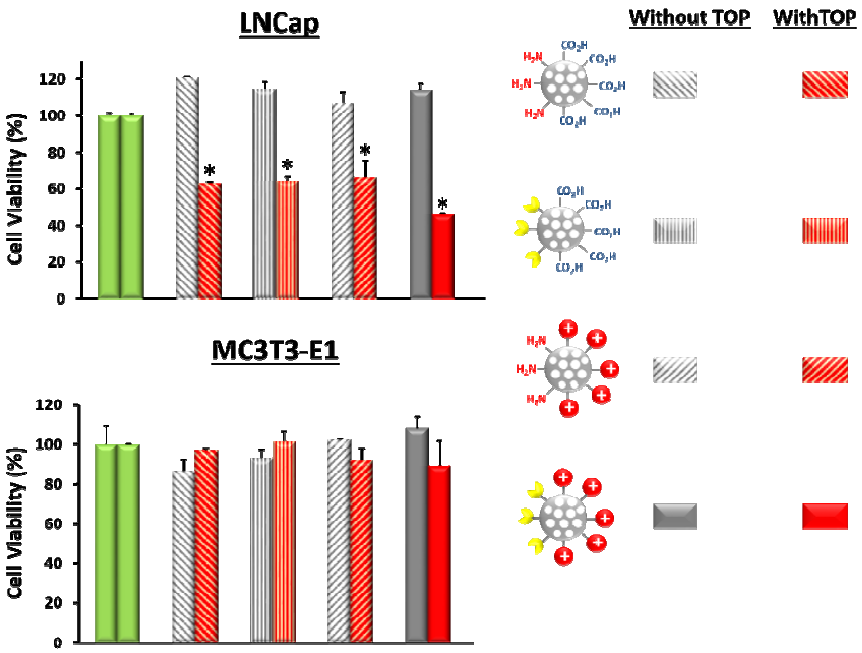

Figure 6. Cell viability studies with and without TOP loaded within the MSN for LNCaP (up) and MC3T3-E1 (down) cell lines, respectively and 48 hours of exposition time. *$p < 0.05$ vs. corresponding control without TOP (Student's t-test).

In a parallel way, the capacity of these materials to deliver cytotoxic drugs in a selective manner to tumoral cells was evaluated employing MSN loaded with a cytotoxic compound, in this case topotecan (TOP). TOP is an inhibitor of DNA topoisomerase-I, which is an enzyme in charge to reduce the strain in the DNA chains during replication. The administration of this drug induces damages in the DNA located in the cell nucleus and also in the mitochondria causing the cell death. This drug present high antitumoral activity but it suffers instability at neutral and basic pH, losing its activity after few hours.[35] Therefore, it is needed to administrate repeated dosages of this drug in order to maintain its concentration in blood, which induces the apparition of systemic toxicity. For these facts, TOP has been selected as drug model for this system. Thus, TOP was loaded within MSN derivatives by soaking the particles in a saturated aqueous solution of TOP (3 $mg \cdot mL^{-1}$). The amount of loaded TOP was determined by the difference in fluorescent

of the loading solution before and after the MSN immersion, showing in all cases around 5% of TOP in weight. LNCap and MC3T3-E1 cells were exposed to a fixed concentration of TOP-loaded MSN during 6 hours. After this time, the cells were gently washed with PBS in order to remove the non-internalized particles and they were incubated 48 hours more in cell culture medium. In the case of tumoral cell line, when cells were exposed to untargeted MSN or mono-functionalized targeted MSN (MSN-Fol and MSN-TPP), cell viability descended around 35-40% in all cases (Fig. 6). Cell viability decrease was significantly higher in the case of dual-targeted MSN (Fol-MSN-TPP) which shows around 55% of cell viability reduction. The higher toxicity can be attributed to the enhanced uptake observed and also to the close proximity of the nanocarrier to mitochondria, which could enhance the efficacy of the released TOP, as has been described in other systems.[36] It is important to point out that the particle concentration in all cases were very low (6 μg·mL-1) and the exposition time in each case were also short (6 hours), which indicate the great cytotoxic capacity of these nanocarriers. In the case of healthy cells, only a slight decrease in cell viability was observed in the case of dual-targeted MSN (11%). This fact can be attributed to the lower uptake observed in these cells in comparison with the tumoral cell line and also to the higher resistance of healthy cells to cytotoxic drugs.

These data confirm the best performance of dual-targeted MSN in comparison with the mono-functionalized ones, which indicates the excellent suitability of this strategy to enhance the efficacy of nanocarrier-based therapies.

CONCLUSIONS

In this work, a new strategy for the synthesis of asymmetrically functionalized dual targeted MSN has been presented. This method, based on the formation of Pickering emulsions, allows

the obtaining of large amounts of J-MSN which is a significant advantage compared with other reported procedures such as sputter coating or microfluidic techniques. As a proof of concept, folic acid and a triphenylphosphine derivative have been chosen as cellular and organelle targeting moieties, respectively, in order to study the effect of the asymmetric introduction of these groups on the particle surface. The achieved results indicate that the combination of both targeting agents each of them located in one hemisphere of the particle enhances their uptake in tumoral cells and induces the localization of the nanocarrier close to mitochondria which improve the efficacy of the transported drugs. This novel strategy can be easily adapted for the introduction of different targeting moieties on the MSN surface which can improve the arsenal of nanomedicines in the fight against cancer.

ASSOCIATED CONTENT

Supporting Information. The following files are available free of charge. Images of precipitate and supernatant of naked or asymmetrically aminated MSN exposed to gold nanoparticles, location of the MSN nanoparticles in a vial with two phases (organic and aqueous), Hydrodynamic diameter measurements and FTIR spectra of functionalized MSN.

AUTHOR INFORMATION

Corresponding Authors

*Alejandro Baeza, abaezaga@ucm.es; *María Vallet-Regí, vallet@ucm.es

Author Contributions

All authors have given approval to the final version of the manuscript. The manuscript was written through contributions of all authors. V. L[†] and M. R. V[†] have contributed equally. V. R.

has optimized the MSN asymmetrization procedure. G. V has synthesized the TPP analog. D. L. has carried out the cell viability evaluation.

Funding Sources

This work has been done thanks to the financial support provided by European Research Council (Advanced Grant VERDI; ERC-2015-AdG Proposal No. 694160) and the project MAT2015-64831-R.

Notes

The authors declare no competing financial interest

ACKNOWLEDGMENT

This work was supported by the European Research Council (Advanced Grant VERDI; ERC-2015-AdG Proposal No. 694160) and the project MAT2015-64831-R.

REFERENCES

(1) Matsumura, Y.; Maeda, H. A New Concept for Macromolecular Therapeutics in Cancer-Chemotherapy - Mechanism of Tumoritropic Accumulation of Proteins and the Antitumor Agent Smancs. *Cancer Res.* **1986**, *46*, 6387–6392.

(2) Nakamura, H.; Jun, F.; Maeda, H. Development of next-Generation Macromolecular Drugs Based on the EPR Effect : Challenges and Pitfalls. *Expert Opin. Drug Deliv.* **2015**, *12*, 53–64.

(3) Ediriwickrema, A.; Saltzman, W. M. Nanotherapy for Cancer: Targeting and Multifunctionality in the Future of Cancer Therapies. *ACS Biomater. Sci. Eng.* **2015**, *1*, 64–78.

(4) Jain, R. K.; Stylianopoulos, T. Delivering Nanomedicine to Solid Tumors. *Nat. Rev. Clin. Oncol.* **2010**, *7*, 653–664.

(5) Egeblad, M.; Nakasone, E. S.; Werb, Z. Tumors as Organs: Complex Tissues That Interface with the Entire Organism. *Dev. Cell* **2010**, *18*, 884–901.

(6) Vivek, R.; Thangam, R.; Nipunbabu, V.; Rejeeth, C.; Sivasubramanian, S.; Gunasekaran, P.; Muthuchelian, K.; Kannan, S. Multifunctional HER2-Antibody Conjugated Polymeric Nanocarrier-Based Drug Delivery System for Multi-Drug-Resistant Breast Cancer Therapy. *ACS Appl. Mater. Interfaces* **2014**, *6*, 6469–6480.

(7) Lao, Y.; Phua, K. K. L.; Leong, K. W. Aptamer Nanomedicine for Cancer Therapeutics : Barriers and Potential for Translation. *ACS Nano* **2015**, *9*, 2235–2254.

(8) Vlashi, E.; Kelderhouse, L. E.; Sturgis, J. E.; Low, P. S. Effect of Folate-Targeted Nanoparticle Size on Their Rates of Penetration into Solid Tumors. *ACS Nano* **2013**, *7*, 8573–8582.

(9) Field, L. D.; Delehanty, J. B.; Chen, Y.; Medintz, I. L. Peptides for Specifically Targeting Nanoparticles to Cellular Organelles: Quo Vadis ? *Acc. Chem. Res.* **2015**, *48*, 1380–1390.

(10) Villaverde, G.; Baeza, A.; Melen, G. J.; Alfranca, A.; Ramirez, M.; Vallet-Regí, M. A New Targeting Agent for the Selective Drug Delivery of Nanocarriers for Treating Neuroblastoma. *J. Mater. Chem. B* **2015**, *3*, 4831–4842.

(11) Zhao, Y.; Jiang, Y.; Lv, W.; Wang, Z.; Lv, L.; Wang, B.; Liu, X.; Liu, Y.; Hub, Q.; Sun, W.; Xu, Q. Xin, H.; Gu, Z. Dual Targeted Nanocarrier for Brain Ischemic Stroke Treatment. *J. Control. Rel.*, **2016**, 233, 64-71.

(12) Li, Y.; Hea, H.; Jia, X.; Lu, W-L.; Lou, J.; Wei, Y. A Dual-targeting Nanocarrier Based on Poly(amidoamine) Dendrimers Conjugated with Transferrin and Tamoxifen for Treating Brain Gliomas. *Biomaterials*, **2012**, 33, 3899-3908.

(13) Pan, W.; Yang, H.; Zhang, T.; Li, Y.; Li, N.; Tang, B. Dual-targeted Nanocarrier Based on Cell Surface Receptor and Intracellular mRNA: An Effective Strategy for Cancer Cell Imaging and Therapy. *Anal. Chem.* **2013**, 85, 6930−6935.

(14) Kang, B. H.; Plescia, J.; Song, H. Y.; Meli, M.; Colombo, G.; Beebe, K.; Scroggins, B.; Neckers, L.; Altieri, D. C. Combinatorial Drug Design Targeting Multiple Cancer Signaling Networks Controlled by Mitochondrial Hsp90. *J. Clin. Invest.* **2009**, *119*, 454-464.

(15) Rajendran, L.; Knölker, H.-J.; Simons, K. Subcellular Targeting Strategies for Drug Design and Delivery. *Nat. Rev. Drug Discov.* **2010**, *9*, 29–42.

(16) Chen, W.-H.; Xu, X.-D.; Luo, G.-F.; Jia, H.-Z.; Lei, Q.; Cheng, S.-X.; Zhuo, R.-X.; Zhang, X.-Z. Dual-Targeting pro-Apoptotic Peptide for Programmed Cancer Cell Death via Specific Mitochondria Damage. *Sci. Rep.* **2013**, *3*, 3468.

(17) Pan, L.; Liu, J.; He, Q.; Shi, J. MSN-Mediated Sequential Vascular-to-Cell Nuclear-Targeted Drug Delivery for Efficient Tumor Regression. *Adv. Mater.* **2014**, *26*, 6742–6748.

(18) Chen, Z.; Zhang, L.; Song, Y.; He, J.; Wu, L.; Zhao, C.; Xiao, Y.; Li, W.; Cai, B.; Cheng, H.; Li, W. Hierarchical Targeted Hepatocyte Mitochondrial Multifunctional Chitosan Nanoparticles for Anticancer Drug Delivery. *Biomaterials* **2015**, *52*, 240–250.

(19) Xia, Q-S; Ding, H-M; Ma, Y-Q. Can Dual Targeting Enhance Cellular Uptake of Nanoparticles? *Nanoscale*, **2017**, *9*, 8982-8989.

(20) Vallet-Regi, M.; Rámila, A.; del Real, R. P.; Pérez-Pariente, J. A New Property of MCM-41: Drug Delivery System. *Chem. Mater.* **2001**, *13*, 308–311.

(21) Vallet-Regí, M.; Balas, F.; Arcos, D. Mesoporous Materials for Drug Delivery. *Angew. Chem. Int. Ed. Engl.* **2007**, *46*, 7548–7558.

(22) Byrne, J. D.; Betancourt, T.; Brannon-Peppas, L. Active Targeting Schemes for Nanoparticle Systems in Cancer Therapeutics. *Adv. Drug Deliv. Rev.* **2008**, *60*, 1615–1626.

(23) Smith, R. a J.; Porteous, C. M.; Gane, A. M.; Murphy, M. P. Delivery of Bioactive Molecules to Mitochondria in Vivo. *Proc. Natl. Acad. Sci. U. S. A.* **2003**, *100*, 5407–5412.

(24) Hattori, Y.; Maitani, Y. Folate-Linked Nanoparticle-Mediated Suicide Gene Therapy in Human Prostate Cancer and Nasopharyngeal Cancer with Herpes Simplex Virus Thymidine Kinase. *Cancer Gene Ther.* **2005**, *12*, 796–809.

(25) Martínez-Carmona, M.; Lozano, D.; Colilla, M.; Vallet-Regí, M. Selective Topotecan Delivery to Cancer Cells by Targeted pH-Sensitive Mesoporous Silica Nanoparticles. *RSC Adv.* **2016**, *6*, 50923–50932.

(26) De la loza Díaz, M. C.; Wellinger, R. E. A Novel Approach for Organelle-Specific DNA Damage Targeting Reveals Different Susceptibility of Mitochondrial DNA to the Anticancer Drugs Camptothecin and Topotecan. *Nucleic Acids Res.* **2009**, *37*, e26.

(27) Martínez-Carmona, M.; Baeza, A.; Rodriguez-Milla, M. a.; García-Castro, J.; Vallet-Regí, M. Mesoporous Silica Nanoparticles Grafted with a Light-Responsive Protein Shell for Highly Cytotoxic Antitumoral Therapy. *J. Mater. Chem. B* **2015**, *3*, 5746–5752.

(28) Ujiie, H.; Shimojima, A.; Kuroda, K. Synthesis of Colloidal Janus Nanoparticles by Asymmetric Capping of Mesoporous Silica with Phenylsilsesquioxane. *Chem. Commun.*, **2015**, *51*, 3211-3214.

(29) Simmchen, J.; Baeza, A.; Ruiz, D.; Esplandiu, M. J.; Vallet-Regí, M. Asymmetric Hybrid Silica Nanomotors for Capture and Cargo Transport: Towards a Novel Motion-Based DNA Sensor. *Small* **2012**, *8*, 2053–2059.

(30) Perro, A.; Meunier, F.; Schmitt, V.; Ravaine, S. Production of Large Quantities of "Janus" Nanoparticles Using Wax-in-Water Emulsions. *Colloids Surf A Physicochem Eng Asp*. 2009, 332, 57-62.

(31) Yoon, T. J.; Yu, K. N.; Kim, E.; Kim, J. S.; Kim, B. G.; Yun, S. H.; Sohn, B. H.; Cho, M. H.; Lee, J. K.; Park, S. B. Specific Targeting, Cell Sorting, and Bioimaging with Smart Magnetic Silica Core-Shell Nanomaterials. *Small* **2006**, *2*, 209–215.

(32) Sapsford, K. E.; Algar, W. R.; Berti, L.; Gemmill, K. B.; Casey, B. J.; Oh, E.; Stewart, M. H.; Medintz, I. L. Functionalizing Nanoparticles with Biological Molecules: Developing Chemistries That Facilitate Nanotechnology. *Chem. Rev.* **2013**, *113*, 1904–2074.

(33) Zhang, Y.; Shen, Y.; Teng, X.; Yan, M.; Bi, H.; Morais, P. C. Mitochondria-targeting Nanoplatform with Fluorescent Carbon Dots for Long Time Imaging and Magnetic Field-Enhanced Cellular Uptake. *ACS Appl. Mater. Interfases*, **2015**, *7*, 10201-10212.

(34) Lu, J.; Liong, M.; Li, Z.; Zink, J. I.; Tamanoi, F. Biocompatibility, Biodistribution, and Drug-Delivery Efficiency of Mesoporous Silica Nanoparticles for Cancer Therapy in Animals. *Small* **2010**, *6*, 1794–1805.

(35) Herben, V. M.; ten Bokkel Huinink, W. W.; Beijnen, J. H. Clinical Pharmacokinetics of Topotecan. *Clin. Pharmacokinet.* **1996**, *31*, 85–102.

(36) Luo, G.-F.; Chen, W.-H.; Liu, Y.; Lei, Q.; Zhuo, R.-X.; Zhang, X.-Z. Multifunctional Enveloped Mesoporous Silica Nanoparticles for Subcellular Co-Delivery of Drug and Therapeutic Peptide. *Sci. Rep.* **2014**, *4*, 1–10.

An easy method for the synthesis of asymmetrically targeted mesoporous silica nanocarriers able to perform sequential cell-organelle vectorization.